

SYNTHESIS OF Pt(II)-COMPLEXES WITH SYMMETRICAL AND UNSYMMETRICAL GLYOXIMES, THEIR PHYSICAL-CHEMICAL AND BIOLOGICAL STUDY

Csaba VÁRHELYI Jr.^{a*}, Roland SZALAY^b, György POKOL^c,
János MADARÁSZ^c, Laura MARINCAS^a, Raluca-Anca MEREU^a,
Judith MIHÁLY^d, Judit PAPP^e, Melinda SIMON-VÁRHELYI^a,
Róbert TÖTÖS^a, Maria TOMOAI-COTIȘEL^a

ABSTRACT. A series of Pt-complexes of the type [Pt(DioxH)₂L₂], (DioxH= deprotonated diethyl-glyoxime, methyl-pentyl-glyoxime, methyl-propyl-glioxime, L=amine) were synthesized, described and characterized with thermoanalytical (TG-DTG-DTA), spectroscopical (FTIR, ESI-MS, UV-VIS and NMR), powder XRD and AFM methods. The biological activity, especially the antibacterial effect, was also studied. The complexes were tested against selected Gram-positive and Gram-negative bacteria. The thermoanalytical measurements revealed the stability of complexes until 200 °C, which then loose characteristic fragments of their ligands. The spectroscopic data are in accordance with the thermal properties of the samples, confirming their composition. The compounds exhibited antibacterial effect against the bacterial strain studied.

Keywords: Pt(II)-complexes, α -dioxime, amine ligand, thermal properties, spectroscopy, AFM, antimicrobial activity

^a Babeş-Bolyai University, Faculty of Chemistry and Chemical Engineering, Arany J. str. 11, RO-400 028, Cluj-Napoca, Romania.

^b Eötvös Loránd University, Institute of Chemistry, Pázmány Péter sétány 1/A, H-1117, Budapest, Hungary.

^c Budapest University of Technology and Economics, Faculty of Chemical Technology and Biotechnology, Műegyetem rkp. 3, H-1111 Budapest, Hungary.

^d Research Centre for Natural Sciences, Institute of Materials and Environmental Chemistry, Magyar tudósok körútja 2, H-1117 Budapest, Hungary.

^e Babeş-Bolyai University, Faculty of Biology and Geology, Mihail Kogălniceanu str. 1, RO-400084, Cluj-Napoca, Romania.

* Corresponding author: csaba.varhelyi@ubbcluj.ro.



INTRODUCTION

After the discovery of anticancer activity of cisplatin by Barnett Rosenberg, platinum coordination complexes became a very important class of drugs [1]. In recent years other platinum-based drugs have entered in clinical trials, and high efforts have been made to find more active and less toxic agents for cancer treatment in humans [2-5]. The mode of action of platinum based antitumor drugs, such as cisplatin and its analogues, is that they bind to the DNA in cancer cells [6-9]. Many pathogenic bacteria show resistance toward antibiotics, therefore it is necessary to find new compounds to control the multidrug-resistant microorganisms [10-13]. For example, some tetracyclines coordinated to Pt(II) showed improved antimicrobial activity [14]. In order to obtain new Pt(II) metallodrugs as good candidates for anticancer or antimicrobial agents, N donor ligands, such as Schiff-bases [15, 16], aliphatic or aromatic amines, are often used [17-20].

Platinum group metal complexes with α -diimine ligands have been used as photosensitizers in energy conversion and electron transfer, in chemi- and electroluminescent systems, and as probes for heterogeneous binding and dynamics of macromolecular structure [21-24]. Other platinum coordination and organometallic complexes have demonstrated applications in homogeneous catalysis, such as the oxidation of ethanol to acetic acid or acetaldehyde, the oxidation of sulfur dioxide to sulfuric acid and, furthermore, in catalytic combustion, hydrogenation reactions. The rationale in utilization is their ability to catalyze reactions under milder conditions with higher selectivity, compared to other metals, their high stability in various oxidation states, functional-group tolerance, and their highly understood synthetic chemistry [25, 26].

Thermal properties of bioactive compounds are relevant to their future usage, therefore thermal analysis is an appropriate technique to characterize the complexes with biological activity [27-30]. Thermoanalytical methods provide important informations on thermal stability, polymorphic forms or structural changes [31-34], as well as purity of potential new drugs [35-36]. The aim of this study was the synthesis, physical-chemical and antimicrobial characterization of some compounds with general formula $[Pt(DioxH)_2L_2]$. Since the thermal properties of biological active compounds are crucial for their future applications, another aim of this work was the detailed thermal analysis of the synthesized coordination compounds.

IR-spectral measurements

We recorded the mid- and far-IR spectra for our compounds, and the results are summarized in the experimental part. Strong bands related to $\nu_{C=N}$ (1519–1535 cm^{-1}) and ν_{Pt-N} (414–518 cm^{-1}) vibrations appear for all studied compounds, which demonstrate the formation of complexes.

If we compare the spectrum of compounds containing symmetrical and unsymmetrical glyoxime ligands we can observe generally a small shift to smaller values of ν_{Pt-N} , $\nu_{C=N}$ bands in case of the unsymmetrical complexes, which can be explained by electronic effects. For example, in Figures 1 and 2 two IR spectra are presented with the only difference in the dioxime moiety. In case of the symmetrical compound the ν_{Pt-N} band appears at 512 cm^{-1} and in the unsymmetrical one does at 508 cm^{-1} . This difference can be explained with the distortion of the molecule, and the increasing Pt–N distance in case of the unsymmetrical complexes.

In the far-IR range (400–100 cm^{-1}) several deformation vibrations appeared, mostly for the heterocyclic amines and for the N–Pt–N groups (δ_{N-Pt-N} : 324–358 cm^{-1}) [37].

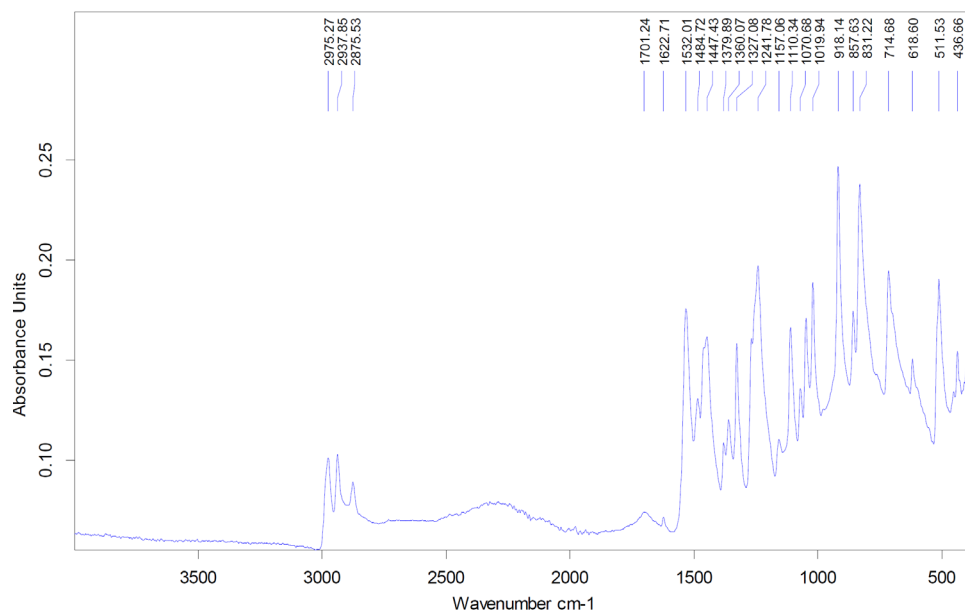


Figure 1. IR spectrum of $[Pt(\text{Diehyl-DioxH})_2(\text{imidazole})_2]$

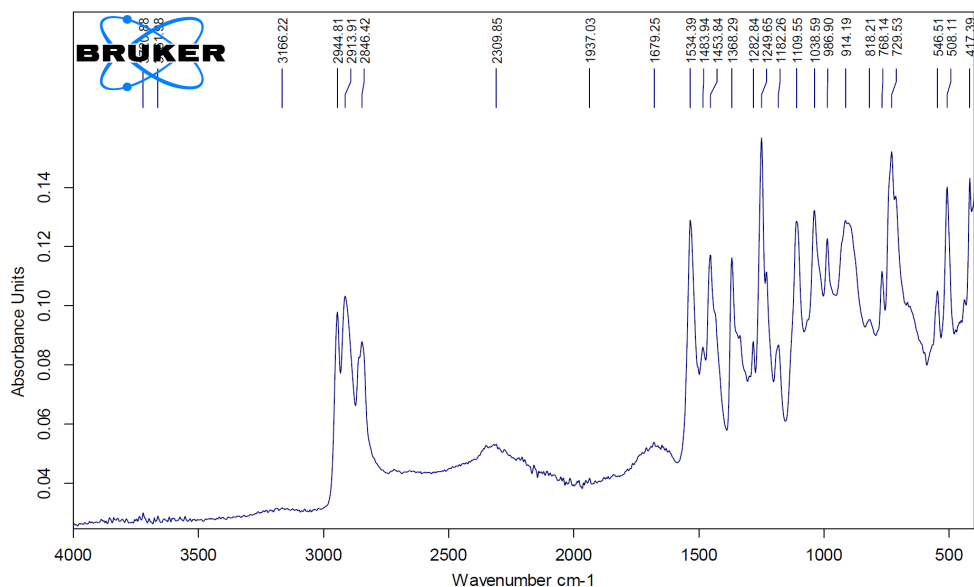


Figure 2. IR spectrum of $[Pt(Me-Pentyl-DioxH)_2(imidazole)_2]$

Raman-spectral measurements

The Raman spectra were recorded in the range of 4000–50 cm⁻¹ for a few complexes exhibiting less dark color. The most important bands appear at the same positions like in the IR spectra but with lower intensities. Due to selection rules in Raman spectroscopy the symmetric vibrations are also detectable which, as a result, can aid the proper assignation of vibrational bands.

Electronic spectra (UV–VIS)

The electronic spectra of some $[Pt(DioxH)_2L_2]$ type complexes were recorded. The free ligand absorption bands appear between 212–286 nm and 320–324 nm which can be assigned to $\pi \rightarrow \pi^*$ transitions of the aromatic rings and $n \rightarrow \pi^*$ transitions of the C=N groups, respectively. A weak band can also be observed between 470–623 nm corresponding to a $d-d$ electron transition that demonstrates a rectangle-planar geometry of glyoxime groups around the metal ion [22]. The calculation of the acidity constants shows that our complexes are weakly acidic due to the deprotonation of the dioximes in basic buffer solutions.

Mass spectrometric measurements

In the mass spectra the molecular ions were successfully detected for all complexes. Table 1 presents the characteristic fragments of complexes. The base peak is generally $[Pt(DioxH)_2]^+$ which indicates the stability of this planar moiety and a weak bonding of Pt to the amines [38].

Table 1. Electrospray mass spectrometric data for $[Pt(DioxH)_2L_2]$ type complexes

Compound	Fragments (m/z)
$[Pt(Diethyl-DioxH)_2]$ (1)	480.9 $[M]^+$, 338.4 $[Pt(Diethyl-DioxH)]^+$, 100.9 $[CH_3-CH_2-C=N-O-O-N]^+$, 60.0 $[N_2O_2]^+$
$[Pt(Diethyl-DioxH)_2(imidazole)_2]$ (2)	617.2 $[M]^+$, 550.9 $[Pt(Diethyl-DioxH)_2(imidazole)]^+$, 480.9 $[Pt(Diethyl-DioxH)_2]^+$, 100.9 $[CH_3-CH_2-C=N-O-O-N]^+$, 60.0 $[N_2O_2]^+$
$[Pt(Diethyl-DioxH)_2(2-amino-pyrimidine)_2]$ (3)	694.8 $[M+Na]^+$, 671.2 $[M]^+$, 481.0 $[Pt(Diethyl-DioxH)_2]^+$, 100.9 $[CH_3-CH_2-C=N-O-O-N]^+$, 60.0 $[N_2O_2]^+$
$[Pt(Diethyl-DioxH)_2(3-aminophenol)_2]$ (4)	722.0 $[M+Na]^+$, 699.0 $[M]^+$, 681.9 $[M-OH]^+$, 665.6 $[M-2OH]^+$, 480.9 $[Pt(Diethyl-DioxH)_2]^+$, 100.9 $[CH_3-CH_2-C=N-O-O-N]^+$, 60.0 $[N_2O_2]^+$
$[Pt(Et-Pr-DioxH)_2(4-amino-3-hydroxynaphthalene-1-sulfonic acid)_2]$ (5)	990.7 $[MH_2]^+$, 830.6 $[Pt(Et-Pr-DioxH)(4-am.-3-hydr.-naph.-1-sulfonic acid)_2]^+$, 510.2 $[Pt(Et-Pr-DioxH)_2]^+$, 434.4 $[Pt(4-am.-3-hydr.-naph.-1-sulfonic acid)]^+$
$[Pt(Et-Pr-DioxH)_2(3-amino-1-propanol)_2]$ (6)	659.7 $[M]^+$, 582.9 $[Pt(Et-Pr-DioxH)_2(3-am.-1-prop)]^+$, 509.3 $[Pt(Et-Pr-DioxH)_2]$
$[Pt(Me-Pentyl-DioxH)_2(imidazole)_2]$ (7)	712.6 $[M+K]^+$, 673.4 $[M]^+$, 657.4 $[M-O]^+$, 605.3 $[Pt(Me-Pentyl-DioxH)_2(imidazole)]^+$, 538.2 $[Pt(Me-Pentyl-DioxH)_2]^+$
$[Pt(Me-Pentyl-DioxH)_2(3-amino-1-propanol)_2]$ (9)	727.6 $[M+K]^+$, 688.5 $[M]^+$, 576.2 $[M-DioxH_2]^+$, 538.2 $[Pt(Me-Pentyl-DioxH)_2]^+$, 428.3 $[Pt(Me-Pentyl-DioxH)_2N_2O_2]^+$
$[Pt(Me-Pentyl-DioxH)_2((n-Bu)_2NH)_2]$ (10)	795.4 $[M]^+$, 779.4 $[M-OH]^+$, 763.4 $[M-OHO]^+$, 538.2 $[Pt(Me-Pentyl-DioxH)_2]^+$, 130.2 $[(n-Bu)_2NH_2]^+$

Thermoanalytical study

The TG, DTG, DTA curves were recorded for the obtained complexes. One example is presented in Fig. 3, and the results for all studied complexes are included in Table 2.

SYNTHESIS OF Pt(II)-COMPLEXES WITH SYMMETRICAL AND UNSYMMETRICAL GLYOXIMES,
THEIR PHYSICAL-CHEMICAL AND BIOLOGICAL STUDY

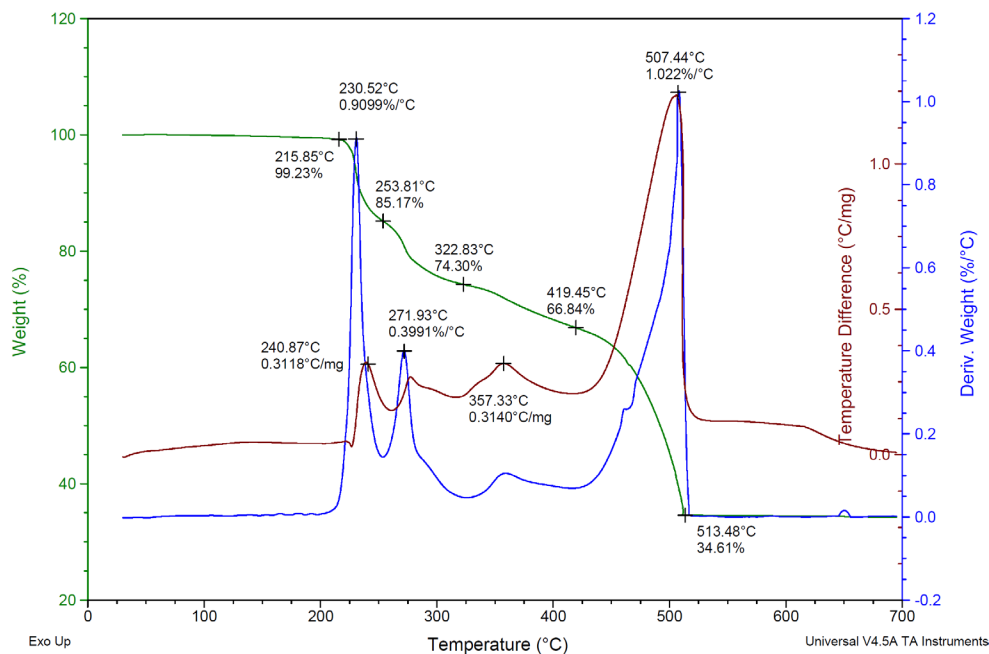


Figure 3. Thermal decomposition curves of $[Pt(\text{DiehyI-DioxH})_2(\text{imidazole})_2]$

The first observation from the thermal decomposition study is the stability of complexes between the temperatures of 115–223 °C. The stability is influenced by the nature of glyoximes and the coordinated amines. Complexes containing symmetrical glyoxime are usually more stable than the unsymmetrical ones (206–223 °C), however, the nature of amines has also influence on the stability. Amines with electron-releasing groups enhance the stability of complexes. The mechanism of the thermal decomposition of complexes was established as well. In the first step the amine elimination takes place until 350 °C, and then the glyoxime groups are leaving until 550 °C which is demonstrated with a big exothermic peak on the DTA curve.

The general decomposition mechanism of $[Pt(\text{DioxH})_2L_2]$ type complexes is shown below:

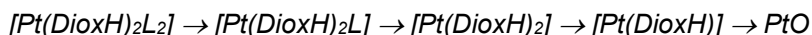


Table 2. Thermoanalytical data of $[Pt(DioxH)_2L_2]$ type complexes

No.	Fragment	t (°C)	m; $-\Delta m$ (%)	DTG (°C)	DTA (°C)
1.	-	206	99.86; 0.14	233.83	238.07 (ex.)
	Diethyl-DioxH	304	66.3; 33.56	274.08	297.39 (ex.)
	Diethyl-DioxH	557	35.96; 30.34	501.48	501.48 (ex.)
	PtO (rest)	695	35.06		
2.	-	216	99.23; 0.77		
	imidazole	254	85.17; 14.06	230.52	240.87 (ex.)
	imidazole	323	74.30; 10.87	271.93	357.33 (ex.)
	2 (Diethyl-DioxH) PtO (rest)	513 513	34.61; 39.69 34.61	507.44	507.44 (ex.)
3.	-	223	99.76; 0.24		
	2 (2-am.-pyrimidine)	293	72.54; 27.22	279.69	302.98 (ex.)
	2 (Diethyl-DioxH)	351	38.11; 34.33	340.94	340.94 (ex.)
	PtO (rest)	689	36.23		
4.	-	223	99.44; 0.56		
	2 (3-hydroxy-aniline)	307	67.84; 31.6	279.69	292.63 (ex.)
	2 (Diethyl-DioxH)	366	40.41; 27.43	349.57	350.43 (ex.)
	PtO (rest)	693	37.75		
5.	-	219	100; 0		
	-SO ₃ H	266	92.35; 7.65	243.79	247.02 (ex.)
	1-amino-2-HO- naphthalene	350	80.15; 12.2	307.54	314.8 (end.)
	2 (Et-Pr-DioxH) + am.	450	29.79; 50.36	442.3	441.5 (ex.)
	PtO (rest)	992	29.24		
6.	-	154	100; 0	197.8	
	2 (3-am.-1-propanol)	284	79.07; 20.93	259.93	261.54 (ex.)
	2 (Et-Pr-DioxH)	395	35.98; 43.09	358.38	359.19 (ex.)
	PtO (rest)	991	33.8		
7.	-	222	98.94; 1.06		
	2 imidazole	282	85.87; 13.07	260.74	263.97 (ex.)
	2 (Me-Pentyl-DioxH)	382	38.6; 47.27	354.34	355.15 (ex.)
	PtO (rest)	990	35.96		
8.	-	115	99.49; 0.51	205.86	174.39 (end.)
	2(2-am.-Py- midine+Me+pentyl)	239	50.49; 49	257.51	260.74 (ex.)
	2 (DioxH)	386	15.68; 34.81	353.54	351.92 (ex.)
	PtO (rest)	991	13.38		
9.	-	200	97.67; 2.33		
	2 (3-am.-1-propanol)	277	83.67; 14	259.93	260.74 (ex.)
	2 (Me-Pentyl-DioxH)	545	38.07; 45.6	338.21	335.78 (ex.)
	PtO (rest)	990	36.76		
10.	-	217	100; 0		
	2 [(n-Bu) ₂ NH] ₂]	310	84.47; 15.53	259.12	262.35 (ex.)
	2 (Me-Pentyl-DioxH)	387	44.98; 39.49	363.22	362.41 (ex.)
	PtO (rest)	990	42.48		

(See the numbering of complexes in the experimental part or scheme 2!)

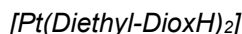
Abbreviations: ex. = exothermic, end. = endothermic

Powder-XRD measurements

The powder-XRD measurements revealed that complexes with symmetrical glyoxime groups show crystalline form with many peaks. However, samples containing unsymmetrical glyoxime groups precipitated out in an amorphous state displaying only some peaks therefore their structure has to be characterized by other methods. The crystalline complexes XRD structures can not be found in the Cambridge Structural Database.

AFM investigations

Two complexes, namely, $[Pt(\text{Diethyl-DioxH})_2]$ and $[Pt(\text{Diethyl-DioxH})_2(2\text{-aminopyrimidine})_2]$ were investigated by atomic force microscopy, and results are presented below.



The film resulting from adsorption is of very good quality, well structured to AFM investigation. The most representative images resulting from the scanning area of $1\ \mu\text{m} \times 1\ \mu\text{m}$ are presented in Figure 4.

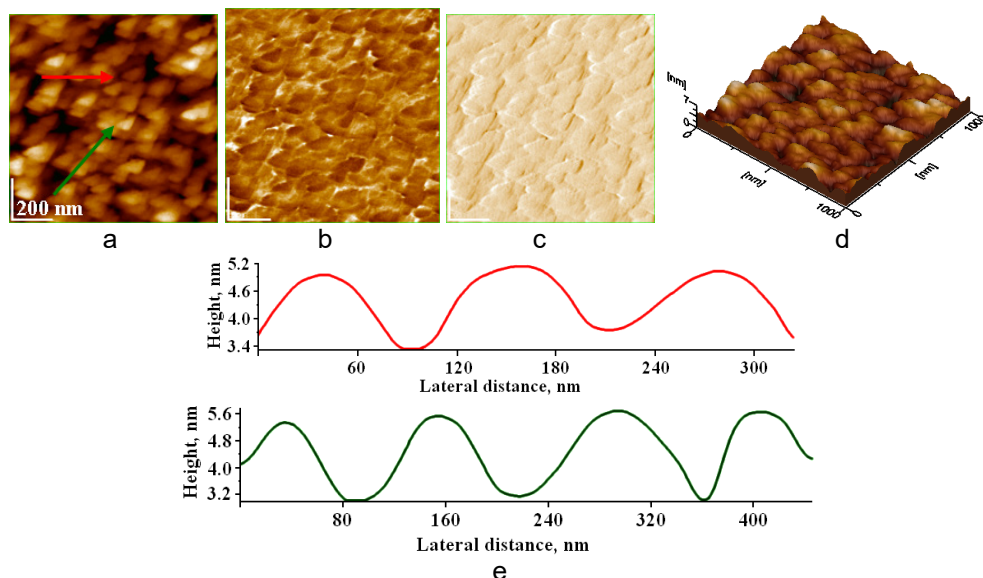
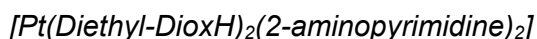


Figure 4. AFM images for $[Pt(\text{Diethyl-DioxH})_2]$: a) topographic image, b) phase image, c) amplitude image, d) 3D image, e) profiles along the arrows in image (a). Scanning area $1\ \mu\text{m} \times 1\ \mu\text{m}$

The topography of the surface highlights an uniform deposition with very well individualized nanoparticles. Their shape is partially equiaxial, enough to allow us to speak about their diameter, but edges appear under sharp angle what foreshadow the formation of corners. The fact correlates with a high crystalline aspect of the interior of these nanoparticles. Their appearance would correlate with well-developed and slender XRD maxima.

The phase and amplitude images, Figures 4b and c, highlight with special clarity the individualization of nanoparticles in the deposition film. Its three-dimensional aspect is shown in Figure 4d. The profiles in Figure 4e indicate a middle diameter of the nanoparticles to be 60 nm.



The deposition film resulting from adsorption has a very good quality too, and lent itself to AFM investigation. The most representative images resulting from the scanning area of $1\ \mu\text{m} \times 1\ \mu\text{m}$ are presented in figure 5.

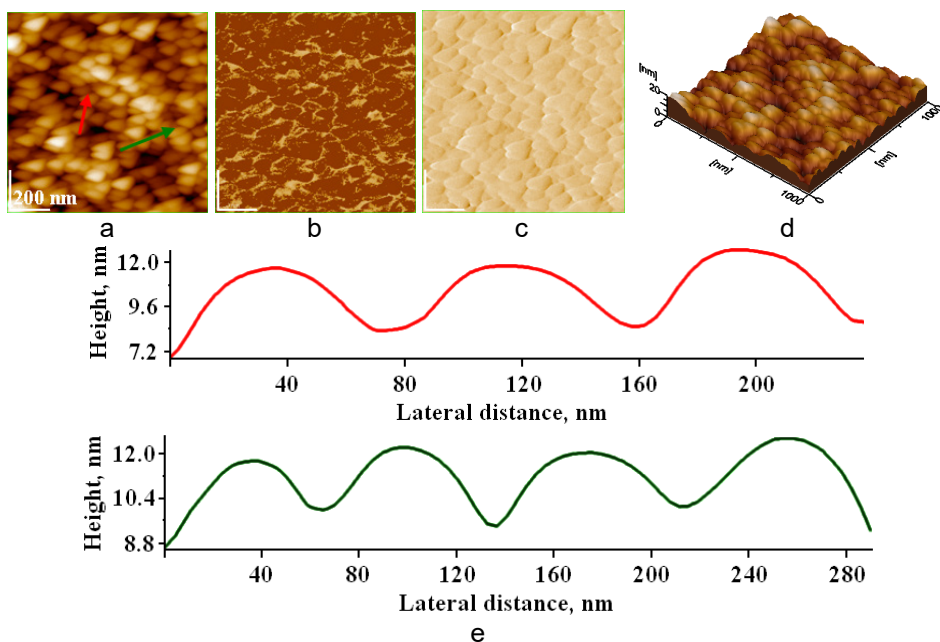


Figure 5. AFM images for $[Pt(Diethyl-DioxH)_2(2\text{-aminopyrimidine})_2]$: a) topographic image, b) phase image, c) amplitude image, d) 3D image, e) profiles along the arrows in image (a). Scanning area $1\ \mu\text{m} \times 1\ \mu\text{m}$

The topographic image, Figure 5a, allows us to visualize the nanoparticles with great clarity. In this way their shape and dimensional aspects, such as the diameter of the nanoparticles can be observed, and the roughness of the deposition can be measured. In the present case we have a fairly uniform film of well-individualized nanoparticles with an equiaxial shape (approximately the same radius in any direction starting from the center of the nanoparticle). Although the observed nanoparticles have a rounded appearance, they are not perfectly spherical due to the fact that their internal crystalline structure leaves its mark to some extent on the external appearance.

In the phase image, Figure 5b, the limit between the nanoparticles appears with a light yellow shade while they have a brown appearance. The fact supports the good individualization of the nanoparticles in the deposition film. The amplitude image, Figure 5c, shows that the sample was scanned under optimal conditions, and the nanoparticles stand out clearly. AFM imaging has the advantage to produce real three-dimensional images due to the scaling in metric units of the Z axis. Therefore, Figure 5d clearly shows the three-dimensional aspect of the deposition and the nanoparticles can be clearly seen how they adsorbed on the glass surface. This deposition is very smooth with a roughness of only 3.18 nm (Table 3). Last but not least, the profiles drawn in Figure 5e allow us to observe the rounded equiaxial aspect of the nanoparticles and thus to determine their diameter accurately. We found that the sample has nanoparticles with a diameter of 40 nm.

Table 3. AFM measured values

Compound	Height (nm)	Rugosity RMS (nm)			Nanopart. diameter (nm)
		Area	Red profile	Green profile	
[Pt(Diethyl-DioxH) ₂] (1)	7	1.09	0.50	0.81	60
[Pt(Diethyl-DioxH) ₂ (2-aminopyrimidine) ₂] (3)	20	3.18	1.37	0.96	40

It is observed that samples with small diameter of nanoparticles lead to the formation of films with lower roughness, while samples with nanoparticles with larger diameters and a very good individualization led to higher values of roughness.

NMR measurements

The NMR spectra of some complexes containing symmetrical and unsymmetrical glyoxime were recorded. In case of the symmetrical glyoximes, in the ¹H NMR spectra the aliphatic protons from the glyoxime

groups appear at 1.1–2.8 ppm in all complexes, and the aromatic protons from the amines appear between 7.7–8.3 ppm. In the ^{13}C NMR spectra the aliphatic carbons appear at 10–20 ppm, and the double bonded carbons appear at 158 ppm. In case of unsymmetrical glyoximes in the ^1H NMR spectra the aliphatic protons from the glyoxime groups appear at 0.8 ppm up to 2,6 ppm on the longer chain. The glyoxime OH protons appear at 11.3–11.4 ppm, the aliphatic amine protons appear between 0.85–2.5 ppm, the amino group protons values are 2.6–8.2 ppm. In case of imidazole group the shift is 8.1 ppm.

Making a comparison between the free ligand and the complex, for example Et-Pr-DioxH₂ and $[\text{Pt}(\text{Et-Pr-DioxH})_2(3\text{-amino-1-propanol})_2]$, a small shift to higher ppm values can be observed in case of the complex (e. g.: from 0.85 ppm to 0.88 ppm – methyl group, from 11.30 ppm to 11.32 ppm – glyoxime OH group). This can be explained with the electron attracting effect of Pt. This effect is reduced by the electron-donor property of the aliphatic amino groups. In case when the amine ligand is aromatic the first peak of methyl group appears at higher value, 1.1 ppm (complexes **1 – 4**).

Adsorption test

The adsorption of $[\text{Pt}(\text{Me-Pentyl-DioxH})_2(\text{imidazole})_2]$ was tested on hydroxyapatite. The adsorption efficiency was 90.5 % and the adsorption capacity 226.36 mg/g, calculated from the calibration straight equation. The OH group of hydroxyapatite and the calcium center serve as active sites for the formation of H-bridge bonds.

Biological assay

The antimicrobial effects of the Pt-complexes were tested against Gram-negative *Serratia marcescens* and Gram-positive *Bacillus subtilis* bacteria. The complexes were dissolved in DMSO, and the concentration was 2 mmol/l. In case of $[\text{Pt}(\text{diethyl-DioxH})_2(\text{imidazole})_2]$ and $[\text{Pt}(\text{diethyl-DioxH})_2(3\text{-hydroxy-aniline})_2]$ the Kirby-Bauer disk diffusion method, while in case of $[\text{Pt}(\text{Et-Pr-DioxH})_2(4\text{-amino-3-hydroxynaphthalene-1-sulfonic acid})_2]$, $[\text{Pt}(\text{Me-Pentyl-DioxH})_2(2\text{-aminopyrimidine})_2]$, $[\text{Pt}(\text{Me-Pentyl-DioxH})_2(3\text{-amino-1-propanol})_2]$ the fluorescein-diacetate (FDA) hydrolysis assay were used for the evaluation of the antibacterial potential. The inhibitory effect of compounds on the development of bacteria was determined by measuring the inhibition zone around the paper discs containing 5 μl , 10 μl , 20 μl or 30 μl of the tested complexes. The spectrophotometrically determined FDA hydrolysis

rate reflect the biofilm-inhibiting effect of the complexes added in different quantities (5 μ l, 10 μ l or 20 μ l) to the nutrient media used for the cultivation of bacteria. The antibacterial effect can be deduced from the absorbance values at 490 nm: the smaller absorbance values indicate a bigger inhibition of the enzyme activity of biofilm-forming bacteria. The degree of inhibition can be calculated in relation to the control sample, which was prepared without Pt-complexes, so the enzyme activity and the biofilm formation was considered 100 %. Each value obtained represents the average of 5 different measurements. The results are included in Table 4 and 5.

Table 4. The dimensions of inhibition zones as a function of the quantity of complexes applied

Compound	5 μ l	10 μ l	20 μ l	30 μ l
[Pt(diethyl-DioxH) ₂ (imidazole) ₂] (2)	-	9 mm	12,7 mm	16,33 mm
[Pt(diethyl-DioxH) ₂ (3-hydroxy-aniline) ₂] (4)	-	7,83 mm	13,66 mm	14,66 mm

Table 5. The inhibition degree of bacterial biofilm-forming capacity ($A_{control} = 1.575$)

Compound	5 μ l/ml		10 μ l/ml		20 μ l/ml	
	A	Inhibition degree (%)	A	Inhibition degree (%)	A	Inhibition degree (%)
[Pt(Et-Pr-DioxH) ₂ (4-amino-3-hydroxynaphthalene-1-sulfonic acid) ₂] (5)	1.235	21.587	1.124	28.635	0.500	68.254
[Pt(Me-Pentyl-DioxH) ₂ (2-amino-pyrimidine) ₂] (8)	1.468	6.794	1.352	14.159	1.327	15.746
[Pt(Me-Pentyl-DioxH) ₂ (3-amino-1-propanol) ₂] (9)	1.458	7.429	1.430	9.206	1.320	16.190

(5, 10 or 20 μ l complex solution was added to 1 ml nutrient broth)

Conclusions

Platinum complexes containing novel N-donor ligands were synthesized, and their structure was characterized by different spectroscopic and diffraction methods. According to the thermoanalytical studies the samples show good thermic stability below 125 °C and their stepwise decomposition mechanism

was also determined. The antibacterial activity of the synthesized compounds was tested against selected bacteria by two microbiological methods providing good inhibition results. In future we also wish to extend our researches to investigate their anti-tumor effect.

EXPERIMENTAL SECTION

The IR spectra of the complexes were recorded with a Bruker Alpha FTIR spectrometer (Platinum single reflection diamond ATR), at room temperature, in the mid-IR (4000–400 cm^{-1}) and far-IR (650–150 cm^{-1}) range, respectively, on a Perkin–Elmer System 2000 FTIR spectrometer, operating with a resolution of 4 cm^{-1} . Raman spectra were measured with a Bio-Rad (Digilab) FT-Raman spectrometer (1064 nm NdYAG laser excitation, 250 mW laser power per sample, 4 cm^{-1} resolution, 512 scan). The electronic-spectra were recorded in aqueous solution of 10^{-4} mol/l concentration with Jasco V-670 Spectrophotometer.

Thermal measurements were performed with a 951 TG and 910 DSC calorimeter (TA Instruments), in Ar or N_2 atmosphere, at a heating rate of 10 $\text{K}\cdot\text{min}^{-1}$ (sample mass 4–10 mg). Mass spectrometric (MS) measurements were carried out by a PE Sciex API 2000 triple quadrupole mass spectrometer, using electrospray ionization (ESI) in the 200–1200 m/z region. By ESI-MS, ionization takes place at milder conditions as compared with classical mass spectrometry, therefore it is more sensible for the detection of single and associated dimer molecular ions and their fragment ions.

The NMR spectra were recorded in DMSO-d^6 in 5 mm tubes at RT on a Bruker DRX 500 spectrometer at 500MHz using TMS as internal reference. The AFM measurements were carried out with a JEOL JSPM 4210 atomic force microscope using NSC 15 Hard cantilevers manufactured by Micromasch Co. Phase and amplitude topographic images were recorded simultaneously.

Synthesis of glyoximes

Diethyl-glyoxime was prepared from 3,4-hexanedione (0.1 mol, 13 ml) reacting with hydroxyl-amine hydrochloride (0.2 mol, 13.9 g) dissolved in 50 ml water. The solution was neutralized with KOH (0.2 mol, 11.2 g). The reaction mixture was heated for 2–3 hours (70–80°C), and then the precipitated product was filtered off. After re-crystallization from EtOH or MeOH, it was dried on air.

Ethyl-propyl-glyoxime and methyl-pentyl-glyoxime were prepared from 3-heptanone and 2-octanone, respectively, by the isonitroso method.

Accordingly, upon cooling (ice + NaCl + H₂O) gaseous ethyl-nitrite was bubbled into a mixture containing 0.5 mol monoketone acidified with 2.5 ml HCl for 2–3 hours. The dion-monoximes as intermediate products were converted to the corresponding dioxime with hydroxyl-amine hydrochloride in the same way as in the diethyl-glyoxime preparation. The crude products were recrystallized from ethyl or methyl alcohol. Yield: 80–90%.

Synthesis of [Pt(DioxH)₂L₂] type complexes

The platinum salt was reduced with formic acid (1 ml for 1.0 mmol PtCl₄) before its use in the complex synthesis (Scheme. 2). 2.0 mmol glyoxime dissolved in EtOH or MeOH (20 ml) was added to the aqueous solution of the reduced platinum salt (PtCl₂, 1.0 mmol). The mixture was heated for 1 hour, and then the corresponding amine (2.0 mmol) was added, and heated further for 2–3 hours. After cooling, the formed complexes were filtered, washed with EtOH–water mixture (1:1), and dried on air. Details of the preparations, yields are given in Table 6.

Table 6. Preparation data for [Pt(DioxH)₂L₂] type derivatives

No.	Starting materials (g; mol)			Product	Yield (g; %)
	PtCl ₄	DioxH ₂	Amine		
1.	0.34; 0.001	diethyl-DioxH ₂ 0.3; 0.002	-	[Pt(di-Et-DioxH) ₂]	0.3; 59
2.	0.34; 0.001	diethyl-DioxH ₂ 0.3; 0.002	imidazole 0.14; 0.002	[Pt(di-Et-DioxH) ₂ (imidazole) ₂]	0.36; 56
3.	0.34; 0.001	diethyl-DioxH ₂ 0.3; 0.002	2-amino-pyrimidine 0.19; 0.002	[Pt(di-Et-DioxH) ₂ (2-aminopyrimidine) ₂]	0.38; 54
4.	0.34; 0.001	diethyl-DioxH ₂ 0.3; 0.002	3-am.-phenol 0.22; 0.002	[Pt(di-Et-DioxH) ₂ (3-aminophenol) ₂]	0.31; 42
5.	0.34; 0.001	Et-Pr-DioxH ₂ 0.32; 0.002	4-amino-3-HO-napht.- 1-sulfonic acid 0.48; 0.002	[Pt(Et-Pr-DioxH) ₂ (4- amino-3-HO-napht.- 1-sulfonic acid) ₂]	0.25; 25
6.	0.34; 0.001	Et-Pr-DioxH ₂ 0.32; 0.002	3-am.-1-propanol 0.15; 0.002	[Pt(Et-Pr-DioxH) ₂ (3- amino-1-propanol) ₂]	0.34; 51
7.	0.34; 0.001	Me-Pent.-DioxH ₂ 0.34; 0.002	imidazole 0.14; 0.002	[Pt(Me-Pentyl- DioxH) ₂ (imidazole) ₂]	0.27; 41
8.	0.34; 0.001	Me-Pent.-DioxH ₂ 0.34; 0.002	2-amino-pyrimidine 0.19; 0.002	[Pt(Me-Pent.-DioxH) ₂ (2-aminopyrimidine) ₂]	0.29; 43
9.	0.34; 0.001	Me-Pent.-DioxH ₂ 0.34; 0.002	3-am.-1-propanol 0.15; 0.002	[Pt(Me-Pent.-DioxH) ₂ (3-am.-1-propanol) ₂]	0.29; 43
10.	0.34; 0.001	Me-Pent.-DioxH ₂ 0.34; 0.002	(n-Bu) ₂ NH 0.26; 0.002	[Pt(Me-Pentil- DioxH) ₂ ((n-Bu) ₂ NH) ₂]	0.41; 52

Analysis

The microscopic appearance studied with an optical microscope and IR-spectral measurement results for the synthesized compounds are given in Tables 7, 8.

Table 7. Microscopic aspect, color and molar mass for $[Pt(DioxH)_2L_2]$ type derivatives

No.	Compound	Molar mass	Color	Microscopic aspect
1.	$[Pt(di-Et-DioxH)_2]$	481.41	Brown	triangle-based prisms
2.	$[Pt(di-Et-DioxH)_2(\text{imidazole})_2]$	617.56	Brown	square-based long crystals
3.	$[Pt(di-Et-DioxH)_2(2\text{-aminopyrimidine})_2]$	671.61	Brown	long needles, triangle-based prisms
4.	$[Pt(di-Et-DioxH)_2(3\text{-aminophenol})_2]$	699.66	Black	shining, triangle-based prisms
5.	$[Pt(Et-Pr-DioxH)_2(4\text{-amino-3-HO-napht.-1-sulfonic acid})_2]$	987,95	Purple	smaller triangle-based prisms
6.	$[Pt(Et-Pr-DioxH)_2(3\text{-amino-1-propanol})_2]$	687,73	Dark purple	triangle-based prisms
7.	$[Pt(Me-Pentyl-DioxH)_2(\text{imidazole})_2]$	673,67	Reddish-brown	needle-like triangle-based prisms
8.	$[Pt(Me-Pent.-DioxH)_2(2\text{-aminopyrimidine})_2]$	727,72	Dark purple	bigger triangle-based prisms
9.	$[Pt(Me-Pent.-DioxH)_2(3\text{-am.-1-propanol})_2]$	687,73	Dark purple	triangle-based prisms
10.	$[Pt(Me-Pentil-DioxH)_2((n-Bu)_2NH)_2]$	796,00	Reddish-brown	thin needle-shaped triangle-based prisms

Electronic spectra (UV–VIS)

As having similar absorption wavelengths and acidity constants the electronic spectra of only some representative $[Pt(DioxH)_2L_2]$ complexes were recorded in aqueous solution containing 10% EtOH. Making a comparison between the free ligand and the complex, for example Et-Pr-DioxH₂ and $[Pt(Et-Pr-DioxH)_2(3\text{-amino-1-propanol})_2]$, a small shift to higher ppm values can be observed in case of the complex (e. g.: from 0.85 ppm to 0.88ppm – methyl group, from 11.30 ppm to 11.32 ppm – glyoxime OH group). This can be explained with the electron attracting effect of Pt. This effect is

reduced by the electron-donor property of the aliphatic amino groups. In case when the amine ligand is aromatic the first peak of methyl group appears at higher value, 1.1 ppm (complexes **1 – 4**). The observed absorption bands are summarized in Table 7. The spectra in Sørensen buffer solution in basic domain [39] were also recorded, and the acidity constants were calculated. The concentration of complexes was $2.8 \cdot 10^{-5}$ mol/l, and the used formula:

$$pK_a = pH + \lg \frac{A - A_{max}}{A_{min} - A}, K_a = 10^{-pK_a},$$

where A – absorbance for the selected pH value, A_{max} – maximum absorbance, A_{min} – minimum absorbance. The acidity constants are summarized in Table 9.

Table 8. FTIR-spectroscopic data

Vibration (cm ⁻¹)	1	2	3	4	5	6	7	8	9	10
ν_{N-H}	-	-	-	3223 w	3196 3098 w	3184 w	3166 w	3188 m	3142 w	3165 w
ν_{C-H}	2975 2938 2876 m	2975 2938 2876 m	2975 2937 2875 m	2974 2937 2876 w	2944 2908 m	3030 2948 2862 m	2945 2914 2846 m	2943 2918 2860 s	2945 2914 2847 m	2944 2916 2848 s
$\nu_{C=C}$	-	1623 w	1670 w	1610 m	1647 m	-	1679 w	1683 w	-	-
$\nu_{C=N}$	1535 s	1532 vs	1535 s	1534 s	1519 vs	1528 vs	1534 vs	1531 s	1534 vs	1527 s
δ_{CH_2}	1459 s	1447 s	1459 s	1448 s	1427 s	1451 vs	1454 s	1442 s	1453 s	1451 s
δ_{CH_3}	1360 m	1360 s	1359 m	1358 w	1347 s	1371 vs	1368 s	1371 s	1369 s	1372 s
ν_{N-O}	1241 vs	1242 vs	1241 vs	1240 vs	1221 s	1238 vs	1250 vs	1247 s	1249 vs	1258 vs
ν_{N-OH}	1107 s	1110 s	1106 s	1106 s	1104 s	1109 vs	1110 vs	1112 m	1110 s	1112 s
τ_{O-H}	916 vs	918 vs	916 vs	915 vs	1044 vs	913 vs	1039 vs	974 vs	1039 s	919 s
γ_{C-H}	712 s	715 s	712 s	710 s	655 vs	739 s	730 vs	726 vs	730 vs	732 vs
ν_{Pt-N}	518 s	515 509 s	518 515 s	513 501 s	519 s	506 434 s	508 417 vs	508 420 m	507 417 vs	511 414 vs
δ_{N-Pt-N}	358 vs	356 vs	328 vs	324 vs	-	-	-	-	-	-

s = strong; vs = very strong; m = medium; w = weak

AFM investigations

In a first phase, an attempt was made to display the samples on a solid support by dispersion in ultrapure water and transfer to the glass surface by vertical adsorption from the aqueous dispersion, but the results obtained were not satisfactory. For this reason, the powdery material was dispersed in DMSO, followed by vertical adsorption on glass slides. Sample drying has been shown to be a primary factor in the success of the AFM investigation. In this sense, we opted for natural drying in a vertical position to facilitate the draining of DMSO excess from the slide before solidification of the deposited film. The adsorption time was 5 s.

Several macroscopically different areas (minimum 5 areas) were scanned on each sample at several scanning areas such as for example 2.5 μm x 2.5 μm to 1 μm x 1 μm . Upon detailed examination of the resulting images, it was observed that the structures on the samples are best highlighted at the 1 μm x 1 μm scan area, revealing the nanostructural aspects of the samples. With the help of the image processing software, JEOL Win SPM Processing 2.0, measurements of surface roughness and profilometry associated with the measurement of the diameters of the nanoparticles in the composition of the samples were performed.

Table 9. Electronic spectral data

Compound	Absorption band (nm)	K_a
[Pt(Diethyl-DioxH) ₂] (1)	271 vs 320 m 470 w	$2.30 \cdot 10^{-10}$
[Pt(Diethyl-DioxH) ₂ (2-aminopyrimidine) ₂] (3)	198 vs 286 m	$3.24 \cdot 10^{-10}$
[Pt(Et-Pr-DioxH) ₂ (3-amino-1-propanol) ₂] (6)	215vs 284 s 324 s 520 m	$7.98 \cdot 10^{-11}$
[Pt(Me-Pentyl-DioxH) ₂ (imidazole) ₂] (7)	212 s 282 s 324 s 623 w	$8.39 \cdot 10^{-12}$

vs = very strong; s = strong; m = medium; w = weak

Adsorption test

For the adsorption test 0.1 g hydroxyapatite was measured and added 5 ml of $[Pt(Me-Pentyl-DioxH)_2(imidazole)_2]$ solution with a concentration of 2 g/l. The mixture was stirred for 24 hours on a magnetic stirrer. At the end of the adsorption time, the solution was centrifuged to ensure that the solid and liquid phases were well separated. After centrifugation, the two phases were separated by decantation, and the liquid phase was analyzed spectrophotometrically.

The measurements were performed with a Jasco V-650 two-way spectrometer. The adsorption was carried out in ethanol, ethanol was also used as a reference solution. Calibration series were prepared. The non-adsorbed complex quantity was calculated from the equation of the calibration line, and from here, knowing the initial concentration, the exact quantity of the adsorbed complex was calculated. The measurements were carried out at wavelength of $\lambda = 330$ nm. The adsorption capacity was determined by using the following formula:

$$q_t = \frac{m_{ads}}{m_{ad}} \left(\frac{mg}{g} \right)$$

where, q – adsorption capacity, m_{ads} – adsorbed quantity of $[Pt(Me-Pentyl-DioxH)_2(imidazole)_2]$ (mg), m_{ad} – quantity of support material (g).

The adsorption efficiency was determined using the following formula:

$$\eta = \frac{c_i - c_f}{c_i} \cdot 100 (\%)$$

where, c_i – initial concentration of $[Pt(Me-Pentyl-DioxH)_2(imidazole)_2]$ (mol/l) and c_f – the $[Pt(Me-Pentyl-DioxH)_2(imidazole)_2]$ concentration at a specific time (mol/l). Using these equations, were obtained the values of adsorption efficiency: 90.5 % and adsorption capacity: 226.36 mg/g [40].

Biological probes

The antimicrobial effects for two complexes were tested by the Kirby-Bauer disk diffusion method, for a Gram-negative (*Serratia marcescens*) bacteria. The tested bacterial suspension was spread on nutrient agar medium, then sterile filter paper disks, containing 5 μ l, 10 μ l, 20 μ l or 30 μ l of the sample solution (2 mmol/l) were added. After incubation (24 hour at 37 °C) the diameter of inhibition zones were measured.

Other complexes were studied for biofilm-inhibiting effect in case of the Gram-positive bacterium (*Bacillus subtilis*). The antibacterial properties were evaluated spectrophotometrically, based on the fluorescein-diacetate hydrolysis assay.

ACKNOWLEDGEMENT

The authors wish to express their thankfulness to the “Domus Hungarica Foundation” of Hungary for the several fellowships provided to Csaba Várhelyi jr.

REFERENCES

1. N.J. Wheate; S. Walker; G.E. Craig; R. Oun; *Dalton Trans.*, **2010**, *39*, 8113-8127
2. W.A. Wani; S. Prashar; S. Shreaz; S.Gómez-Ruiz; *Coord. Chem. Rev.*, **2016**, *312*, 67-98
3. Z. Wang; M. Wua; S. Gou; *J. Inorg. Biochem.*, **2016**, *157*, 1-7
4. M. Benedetti; F. De Castro; A. Romano; D. Migoni; B. Piccinni; T. Verri; M. Lelli; N. Roveri; F.P. Fanizzi; *J. Inorg. Biochem.*, **2016**, *157*, 73-79
5. B. Mavroidi; M. Sagnou; K. Stamatakis; M. Paravatou-Petsotas; M. Pelecanou; C. Methenitis; *Inorg. Chim. Acta*, **2016**, *444*, 63-75
6. L. Kelland; *Nature Reviews Cancer*, **2007**, *7*, 573-584
7. J. Chen; K. Li; S. Swavey; K.M. Church; *Inorg. Chim. Acta*, **2016**, *444*, 76-80
8. M. Gaber; H.A. El-Ghamry; S.K. Fathalla; *Spectrochim. Acta, Part A*, **2015**, *139*, 396-404
9. E.O. Gulumsek; E.E. Baykal; C. Kucukpolat; E. Onal; P. Balcik-Ercin; T. Yagci; V. Ahsen; A.G. Gurek; *J. Coord. Chem.*, **2022**, *75(1-2)*, 197-210
10. A.R. Timerbaev; C.G. Hartinger; S.S. Aleksenko; B.K. Keppler; *Chem. Rev.*, **2006**, *106*, 2224-2248
11. N.T. Zanvettor; D.H. Nakahata; R.E.F. de Paiva; M.A. Ribeiro; A. Cuin; P.P. Corbi; A.L.B. Formiga; *Inorg. Chim. Acta*, **2016**, *443*, 304-315
12. W. Saenger; P. Orth; C. Kisker; W. Hillen; W. Hinrichs; *Angew. Chem. Int. Ed. Engl.*, **2000**, *39*, 2042-2052
13. B.S. Speer; N.B. Shoemaker; A.A. Salyers; *Clinical Microbiol. Rev.*, **1992**, *5*, 387-399
14. W. Guerra; I.R. Silva; E.A. Azevedo; A.R. de S. Monteiro; M. Bucciarelli-Rodriguez; E. Chartone-Souza; J.N. Silveira; A.P.S. Fontes; E.C. Pereira-Maia; *J. Braz. Chem. Soc.*, **2006**, *17*, 1627-1633
15. C. Shiju; D. Arish; N. Bhuvanesh; S. Kumaresan; *Spectrochim. Acta, Part A*, **2015**, *145*, 213-222
16. F.U. Rahman; A. Ali; I. Khan; R. Guo; L. Chen; H. Wang; Z.T. Li; Y. Lin; D.W. Zhang; *Polyhedron*, **2015**, *100*, 264-270

SYNTHESIS OF Pt(II)-COMPLEXES WITH SYMMETRICAL AND UNSYMMETRICAL GLYOXIMES,
THEIR PHYSICAL-CHEMICAL AND BIOLOGICAL STUDY

17. A.M. Mansour; N.T. Abdel-Ghani; *Inorg. Chimica Acta*, **2015**, 438, 76-84
18. N.T. Abdel-Ghani; A.M. Mansour; *J. Mol. Struct.*, **2011**, 991, 108-126
19. S.J. Sabounchei; P. Shahriary; S. Salehzadeh; Y. Gholiee; A. Chehregani; *Comptes Rendus Chimie*, **2015**, 18, 564-572
20. S.J. Sabounchei; P. Shahriary; S. Salehzadeh; Y. Gholiee; D. Nematollahi; A. Chehregani; A. Amani; Z. Afsartala; *Spectrochim. Acta, Part A*, **2015**, 135, 1019-1031
21. J.N. Demas; B.A. DeGraff; *Coord. Chem. Rev.*, **2001**, 211, 317-351
22. P. Deveci; B. Taner; Z. Kilic; A. O. Solak; U. Arslan; E. Ozcan; *Polyhedron*, **2011**, 30, 1726-1731
23. M.Z. Shafikov; A.F. Suleymanova; R.J. Kutta; F. Brandl; A. Gorski; R. Czerwiec; *J. Mater. Chem. C*, **2021**, 9, 5808-5818
24. H.Y. Ku; B. Tong; Y. Chi; Y. Chi; C.C. Yeh; C.H. Chang; G.H. Lee; *Dalton Transactions*, **2015**, 44(18), 8552-8563
25. P.B. Kettler; *Org. Proc. Res. Develop.*, **2003**, 7, 342-354
26. J.M. Gichumbi. H.B. Friedrich; *J. Organomet. Chem.*, **2018**, 866, 123-143
27. A.M. Mansour; *J. Thermal Anal. Calorim.*, **2016**, 123, 571-581
28. M.H. Soliman; A.M.M. Hindy. G.G. Mohamed; *J. Thermal Anal. Calorim.*, **2014**, 115, 987-1001
29. E.M. Zayed; M.A. Zayed; A.M.M. Hindy; *J. Thermal Anal. Calorim.*, **2014**, 116, 391-400
30. S. Arora; D. K. Aneja; M. Kumar; C. Sharma; O. Prakash; *J. Thermal Anal. Calorim.*, **2013**, 111, 17-25.
31. D. Giron; *J. Thermal Anal. Calorimetry*, **2001**, 64, 37-60
32. C. Schmidt; N. Senfter; U. J. Griesser; *J. Thermal Anal. Calorimetry*, **2003**, 73, 397-408
33. M.I. Noordin; L.Y. Chung; *J. Thermal Anal. Calorimetry*, **2009**, 95, 891-894
34. B. Holló; J. Magyari; V. Živković-Radovanović; G. Vučković; Z. D. Tomić; I. M. Szilágyi; G. Pokol; K. Mészáros-Szécsényi; *Polyhedron*, **2014**, 80, 142-150
35. D. Giron; C. Goldbronn; *J. Thermal Anal. Calorimetry*, **1995**, 47, 217-251
36. V. Todeschini; P.R. de Oliveira; L.S. Bernardi; R.L. Pereira; C.E.M. de Campos; M.A.S. Silva; N.M. Volpato; *J. Thermal Anal. Calorimetry*, **2014**, 115, 2295-2301
37. K. Nakamoto; *Infrared and Raman spectra of inorganic and coordination compounds*, Part B, 5th Ed. J. Wiley, New York, **1997**
38. J.T. Watson; *Introduction to Mass Spectrometry*, Ed. Racon, New York, **1985**
39. L. Mázor; *Analitikai zsebkönyv*, Műszaki könyvkiadó. Budapest, **1971**, pp. 394
40. R. Barabás; N.I. Farkas; Cs. L. Nagy; O. Cadar; C. Moisa; L. Bizo; *Ceramics International*, **2021**, 47 (6), 8584-8592

